

Deep Transfer Learning for Automated Diagnosis of Skin Lesions from Photographs

Doyoon Kim*

Cleveland High School
California, US
doyoondeankim@gmail.com

Emma Rocheteau†*

Department of Computer Science and Technology
University of Cambridge, UK
ecr38@cam.ac.uk

Abstract

Melanoma is the most common form of skin cancer worldwide. Currently, the disease is diagnosed by expert dermatologists, which is costly and requires timely access to medical treatment. Recent advances in deep learning have the potential to improve diagnostic performance, expedite urgent referrals and reduce burden on clinicians. Through smart phones, the technology could reach people who would not normally have access to such healthcare services, e.g. in remote parts of the world, due to financial constraints or in 2020, COVID-19 cancellations. To this end, we have investigated various transfer learning approaches by leveraging model parameters pre-trained on ImageNet with finetuning on melanoma detection. We compare EfficientNet, MnasNet, MobileNet, DenseNet, SqueezeNet, ShuffleNet, GoogleNet, ResNet, ResNeXt, VGG and a simple CNN with and without transfer learning. We find the mobile network, EfficientNet (with transfer learning) achieves the best mean performance with an area under the receiver operating characteristic curve (AUROC) of 0.931 ± 0.005 and an area under the precision recall curve (AUPRC) of 0.840 ± 0.010 . This is significantly better than general practitioners (0.83 ± 0.03 AUROC) and dermatologists (0.91 ± 0.02 AUROC).

1 Introduction

Melanoma is the most common skin cancer worldwide, and one of the most aggressive [29]. In the United States alone, it is estimated that there will be 100,350 cases and 6,850 melanoma-related deaths in 2020 [2]. Initially, it develops in melanocytes where genetic mutations lead to unregulated growth and the ability to metastasise to other areas of the body [40]. Like many cancers, early detection is key to successful treatment. If melanoma is detected before spreading to the lymph nodes, the average five-year survival rate is 98%. However, this drops to 64% if it has spread to regional lymph nodes, and 23% if it has reached distant organs.

Currently, melanoma is diagnosed by professional medical examination [15]. A meta-analysis conducted by Phillips et al. [25] showed that when distinguishing between melanoma and benign skin lesions, primary care physicians (10 studies) achieve an area under the receiver operating characteristic curve (AUROC) of 0.83 ± 0.03 , and dermatologists (92 studies) achieve 0.91 ± 0.02 .

Recent advances in deep learning have the potential to improve diagnostic performance and improve access to care for those in need [5]. Through mobile application technology, it will soon be possible to diagnose, refer and provide follow-ups to patients in the community. However, worrying findings from Kassianos et al. [13] suggest the majority (if not all) diagnostic applications on app stores have not been clinically validated. As a result, clinicians are becoming increasingly concerned about misleading applications [37]. However, we believe that when models are developed collaboratively with

*Equal contribution, †Corresponding author

clinicians, and when they are rigorously evaluated with significance testing and model interpretability, useful tools can be produced to support health in the community.

In this work, we investigate transfer learning with various Convolutional Neural Networks (CNNs) on the binary classification task of classifying melanoma and benign skin lesions. In addition, we perform post-hoc visualisation of the feature attributions using integrated gradients [33].

2 Related Work

Recent work by Raghu et al. [26] cast doubt on the usefulness of transfer learning (TL) for medical imaging. However, a few TL works have achieved success on the problem of melanoma detection [9, 22, 23, 27, 39, 41] (although they do not necessarily compare the model with and without TL). We did not find an extensive survey on existing TL models such as ours. The highest AUROC for melanoma detection that we found on plain photographs was 0.880 in Bisla et al. [3], which is still lower than the performance for professional dermatologists found in Phillips et al. [25].

3 Methods

Our task is to classify between benign nevi and malignant melanomas. For each patient we have a photograph in RGB format, $\mathbf{x} \in \mathbb{R}^{3 \times 224 \times 224}$ and static features, $\mathbf{s} \in \mathbb{R}^3$ (age, gender and location on the body) and the binary label $y \in \mathbb{R}^1$. Figure 1 shows the basic architecture of all models. Our code is publicly available at https://github.com/aimadeus/Transfer_learning_melanoma.

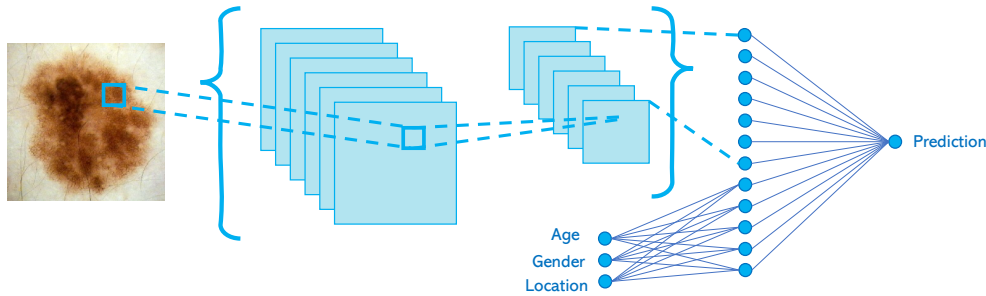


Figure 1: Model architecture. The CNN component (indicated in brackets) is different in each experiment. The static data is processed separately and concatenated to the CNN output before a final prediction is made.

3.1 Transfer Learning

Transfer Learning (TL) is a machine learning method where the weights of a trained model are used to initialise another model on a different task [35]. In our case, we investigate several CNN architectures using pre-training on ImageNet [4] (a database containing over 14 million images). The last fully connected layer is replaced with one that has a binary output, and whose weights are initialised using Kaiming initialisation [7]. Further description of the various CNN architectures are provided in Appendix A. We also train a standard 5-layer CNN with no transfer learning (hyperparameter optimisation and further implementation details are provided in Appendix B and C respectively).

4 Experiments

4.1 Data

We use the International Skin Imaging Collaboration (ISIC) 2020 dataset [28] (released August 2020), containing labelled photographs taken from various locations on the body (see Table 3 in the Appendix). We noted a significant class imbalance with only 2% of the data containing melanoma. To improve this ratio, we added a second dataset with additional malignant cases [1], which brought the total to 37,648 skin lesion images. The data was split such that 60%, 20% and 20% was used for training, validating and testing respectively. Data Augmentation was performed on the training data to introduce small variations in the form of random rotations, horizontal and vertical flipping,

resizing, brightness, and saturation shifts. This means the training data is subtly altered each time it is presented to the model. Figure 2 shows two examples of raw and augmented images respectively.

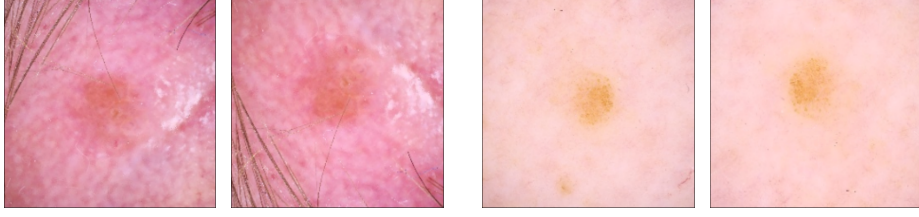


Figure 2: Example photographs in the training data. In each pair of images, the raw data is shown on the left and an augmented image example is shown on the right.

4.2 Results

Table 1 shows the test performance of all the models ((a) without and (b) with transfer learning). Eight of the ten CNN models performed significantly better with TL across all 4 metrics, and none of the models are significantly harmed by TL on any metric, demonstrating a clear benefit of transfer learning for melanoma detection. The best performing models are EfficientNet [18] and MnasNet [36], which significantly outperform dermatologists [25] on AUROC. From the ROC curves shown in Figure 3, we see that the EfficientNet can achieve a true positive rate of 0.95 while only conceding 0.1 to the false positive rate.

Table 1: Performance of the models averaged over 10 independent training runs. Tables (a) and (b) show the performance without and with transfer learning respectively. The error margins are 95% confidence intervals (CIs). We report the accuracy, area under the receiver operating characteristic curve (AUROC), area under the precision recall curve (AUPRC) and the F1 Score. Within each table, the results are ordered from least to best performance. In table (b), if the result is statistically better than the model without transfer learning in a one-tailed t-test ($p < 0.05^*$ and $p < 0.001^{**}$), then it is indicated with stars. Results that significantly outperform general practitioners and dermatologists on AUROC (determined by a recent meta-analysis[†] [25]) are indicated in **green** and **blue** respectively ($p < 0.05$).

	Model	Accuracy	AUROC	AUPRC	F1 Score
(a)	Standard CNN	0.914±0.004	0.759±0.030	0.484±0.026	0.633±0.035
	General Practitioners [†]	-	0.83±0.03	-	-
	VGG [31]	0.943±0.004	0.832±0.018	0.643±0.025	0.765±0.023
	SqueezeNet [11]	0.949±0.003	0.860±0.014	0.687±0.011	0.801±0.008
	ResNeXt [38]	0.952±0.009	0.878±0.022	0.712±0.035	0.818±0.023
	DenseNet [10]	0.957±0.003	0.859±0.015	0.733±0.021	0.824±0.018
	GoogleNet [34]	0.957±0.004	0.861±0.018	0.732±0.024	0.824±0.022
	ResNet-50 [6]	0.959±0.003	0.869±0.016	0.744±0.018	0.835±0.016
	MobileNet [30]	0.963±0.003	0.889±0.013	0.769±0.019	0.856±0.014
	MnasNet [36]	0.963±0.008	0.900±0.010	0.771±0.039	0.859±0.023
	ShuffleNet [19]	0.965±0.004	0.892±0.016	0.777±0.025	0.861±0.018
	EfficientNet [18]	0.967±0.002	0.900±0.009	0.794±0.013	0.872±0.010
(b)	Dermatologists [†]	-	0.91±0.02	-	-
	General Practitioners [†]	-	0.83±0.03	-	-
	VGG [31]	0.959±0.003**	0.874±0.013**	0.740±0.016**	0.835±0.013**
	ResNet-50 [6]	0.962±0.004	0.880±0.014	0.763±0.022	0.849±0.017
	ShuffleNet [19]	0.963±0.006	0.896±0.024	0.769±0.040	0.857±0.028
	SqueezeNet [11]	0.963±0.004**	0.902±0.015**	0.771±0.020**	0.861±0.015**
	DenseNet [10]	0.966±0.003**	0.904±0.011**	0.786±0.018**	0.870±0.011**
	Dermatologists [†]	-	0.91±0.02	-	-
	MobileNet [30]	0.969±0.002**	0.916±0.007**	0.806±0.015**	0.884±0.009**
	ResNeXt [38]	0.971±0.001**	0.918±0.006**	0.819±0.009**	0.891±0.005**
	GoogleNet [34]	0.973±0.002**	0.921±0.006**	0.831±0.013**	0.898±0.008**
	MnasNet [36]	0.974±0.002*	0.928±0.005**	0.832±0.013**	0.901±0.007**
	EfficientNet [18]	0.975±0.002**	0.931±0.005**	0.840±0.010**	0.906±0.006**

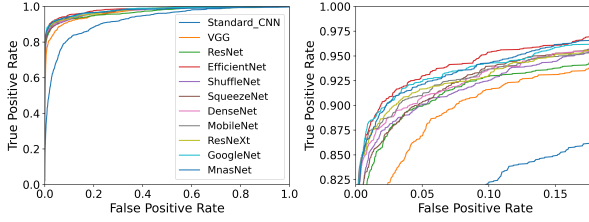


Figure 3: ROC curves of TL models and Standard CNN (we magnify the top left part of the curves in the right plot).

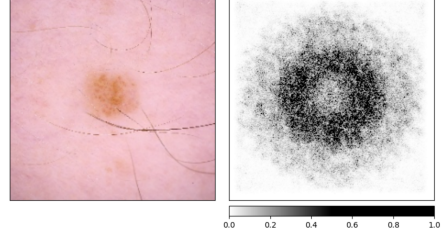


Figure 4: A test set image and corresponding integrated gradient attributions for the standard CNN model.

4.3 Visualisation

We used the integrated gradients method [33] to calculate feature attributions. This method computes the importance scores ϕ_i^{IG} by accumulating gradients interpolated between a baseline \mathbf{b} input (intended to represent the absence of data, in our case this is a black image) and the current input \mathbf{x} .

$$\phi_i^{IG}(\psi, \mathbf{x}, \mathbf{b}) = \underbrace{(\mathbf{x}_i - \mathbf{b}_i)}_{\text{diff. from baseline}} \times \int_{\alpha=0}^1 \underbrace{\frac{\delta\psi(\mathbf{b} + \alpha(\mathbf{x} - \mathbf{b}))}{\delta\mathbf{x}_i}}_{\text{acc. local grad.}} d\alpha \quad (1)$$

The CNN model is represented as ψ^2 . We observed that the models tend to focus primarily on the edges of the skin lesions (Figure 4). This aligns with our expectation, since uneven or notched edges are common in melanoma [20]. Secondary to the edges, there is some importance to the lesion itself and surrounding skin. This is significant because melanomas can also show uneven texture or colour [20].

5 Conclusion

We have conducted an extensive investigation of transfer learning for the task of melanoma detection from photographs. We have demonstrated the benefit of transfer learning with ImageNet pre-training [4] for melanoma detection on the ISIC 2020 dataset [28]. Furthermore, we show that the best performing neural networks are EfficientNet and MnasNet, which are capable of outperforming dermatologists when distinguishing melanoma from benign skin lesions. In particular, we note that these networks have been specifically designed for mobile devices [18, 36]. This may be important when it comes to data privacy and medical data regulations (as the classification can be performed locally on the user’s personal device).

In future work, we plan to investigate the potential of dermoscopy [8] to improve predictions. Secondly, we aim to extend the binary classification task to classify other skin lesions such as benign keratosis, basal cell carcinoma, actinic keratosis, vascular lesions and dermatofibroma. Thirdly, we would like to extend our interpretability study such that we can visualise the learnt features in the intermediate layers of the models. To do this we can leverage the approach of Mordvintsev et al. [21] whereby we obtain inputs designed to maximise the activation of hidden layers of the network. This will provide further insights as to why certain models outperform others in melanoma detection. Finally, we can validate the diagnostic technology in the community with an implementation study.

6 Broader Impact

The automated diagnosis technology could be used to screen, triage, refer and follow-up patients in the community. It also has potential to reach patients who would not normally have access to dermatologists e.g. in remote areas or the developing world. The high AUROC of EfficientNet (high true positive rate coinciding with a low false positive rate) would make it well-suited to this purpose. Such a system could significantly reduce the cost and resources needed to screen and treat as it reduces the pool of patients needing to see the dermatologist.

²The background and intuition behind the method is explained clearly in Sturmfels et al. [32].

References

- [1] melanoma external malignant 256, 2020. URL <https://www.kaggle.com/nroman/melanoma-external-malignant-256>.
- [2] American Cancer Society. Key statistics for melanoma skin cancer, 2020. URL <https://www.cancer.org/cancer/melanoma-skin-cancer/about/key-statistics.html#:~:text=Overall>.
- [3] Devansh Bisla, Anna Choromanska, Jennifer A. Stein, David Polsky, and Russell S. Berman. Skin lesion segmentation and classification with deep learning system. *CoRR*, abs/1902.06061, 2019. URL <http://arxiv.org/abs/1902.06061>.
- [4] J. Deng, W. Dong, R. Socher, L.-J. Li, K. Li, and L. Fei-Fei. ImageNet: A Large-Scale Hierarchical Image Database. In *CVPR09*, 2009.
- [5] Y. Fujisawa, S. Inoue, and Y. Nakamura. The Possibility of Deep Learning-Based, Computer-Aided Skin Tumor Classifiers. *Front. Med.*, 2019.
- [6] K. He, X. Zhang, S. Ren, and J. Sun. Deep residual learning for image recognition. *arXiv 1512.03385*, 12 2015.
- [7] Kaiming He, Xiangyu Zhang, Shaoqing Ren, and Jian Sun. Delving deep into rectifiers: Surpassing human-level performance on imagenet classification. *CoRR*, abs/1502.01852, 2015. URL <http://arxiv.org/abs/1502.01852>.
- [8] G Alden Holmes, Janna M Vassantachart, Brittany A Limone, Michael Zumwalt, Jane Hirokane, and Sharon E Jacob. Using Dermoscopy to Identify Melanoma and Improve Diagnostic Discrimination. *Federal practitioner : for the health care professionals of the VA, DoD, and PHS*, 35(Suppl 4):S39–S45, may 2018. ISSN 1945-337X. URL <https://pubmed.ncbi.nlm.nih.gov/30766399https://www.ncbi.nlm.nih.gov/pmc/articles/PMC6375419/>.
- [9] Khalid M. Hosny, Mohamed A. Kassem, and Mohamed M. Foad. Classification of skin lesions using transfer learning and augmentation with alex-net. *PLOS ONE*, 14(5):1–17, 05 2019. doi: 10.1371/journal.pone.0217293. URL <https://doi.org/10.1371/journal.pone.0217293>.
- [10] G. Huang, Z. Liu, L. van der Maaten, and K. Q. Weinberger. Densely connected convolutional networks, 2018.
- [11] F. N. Iandola, S. Han, M. W. Moskewicz, W. J. Dally K. Ashraf, and Kurt Keutzer. Squeezenet: Alexnet-level accuracy with 50x fewer parameters and <0.5mb model size. *arXiv:1602.07360*, 02 2016.
- [12] Y. Bengio J. Bergstra. Random search for hyper-parameter optimization. *J. Mach. Learn. Res.*, 13:281–305, 02 2012. ISSN 1532-4435.
- [13] A.P. Kassianos, J.D. Emery, P. Murchie, and F.M. Walter. Smartphone applications for melanoma detection by community, patient and generalist clinician users: a review. *British Journal of Dermatology*, 05 2015. doi: 10.1111/bjd.13665.
- [14] Diederik P. Kingma and Jimmy Ba. Adam: A method for stochastic optimization. *CoRR*, abs/1412.6980, 2014.
- [15] H. Kittler, H. Pehamberger, K. Wolff, and M. Binder. Diagnostic accuracy of dermoscopy. *Database of Abstracts of Reviews of Effects (DARE): Quality-assessed Reviews [Internet]*, 2002. URL <https://www.ncbi.nlm.nih.gov/books/NBK69394/>.
- [16] Alex Krizhevsky, Ilya Sutskever, and Geoffrey E Hinton. Imagenet classification with deep convolutional neural networks. In F. Pereira, C. J. C. Burges, L. Bottou, and K. Q. Weinberger, editors, *Advances in Neural Information Processing Systems 25*, pages 1097–1105. Curran Associates, Inc., 2012. URL <http://papers.nips.cc/paper/4824-imagenet-classification-with-deep-convolutional-neural-networks.pdf>.

- [17] Mingchen Li, Mahdi Soltanolkotabi, and Samet Oymak. Gradient descent with early stopping is provably robust to label noise for overparameterized neural networks, 2019.
- [18] Q. V. Le M. Tan. Efficientnet: Rethinking model scaling for convolutional neural networks. *arXiv:1905.11946*, 05 2019.
- [19] N. Ma, X. Zhang, H. Zheng, and J. Sun. Shufflenet v2: Practical guidelines for efficient cnn architecture design. 2018.
- [20] Collette McCourt, Olivia Dolan, and Gerry Gormley. Malignant melanoma: a pictorial review. *The Ulster medical journal*, 83(2):103–110, may 2014. ISSN 2046-4207. URL <https://pubmed.ncbi.nlm.nih.gov/25075139><https://www.ncbi.nlm.nih.gov/pmc/articles/PMC4113154/>.
- [21] Alexander Mordvintsev, Christopher Olah, and Mike Tyka. Inceptionism: Going deeper into neural networks, 2015. URL <https://research.googleblog.com/2015/06/inceptionism-going-deeper-into-neural.html>.
- [22] Dennis H. Murphree and Che Ngufor. Transfer learning for melanoma detection: Participation in ISIC 2017 skin lesion classification challenge. *CoRR*, abs/1703.05235, 2017. URL <http://arxiv.org/abs/1703.05235>.
- [23] Zabir Al Nazi and Tasnim Azad Abir. Automatic skin lesion segmentation and melanoma detection: Transfer learning approach with u-net and dcnn-svm. In Mohammad Shorif Uddin and Jagdish Chand Bansal, editors, *Proceedings of International Joint Conference on Computational Intelligence*, pages 371–381, Singapore, 2020. Springer Singapore. ISBN 978-981-13-7564-4.
- [24] Adam Paszke, Sam Gross, Francisco Massa, et al. PyTorch: An Imperative Style, High-Performance Deep Learning Library. In *Advances in Neural Information Processing Systems 32*, pages 8024–8035. Curran Associates, Inc., 2019.
- [25] Michael Phillips, Jack Greenhalgh, Helen Marsden, and Ioulios Palamaras. Detection of Malignant Melanoma Using Artificial Intelligence: An Observational Study of Diagnostic Accuracy. *Dermatology practical & conceptual*, 10(1):e2020011–e2020011, dec 2019. ISSN 2160-9381. doi: 10.5826/dpc.1001a11. URL <https://pubmed.ncbi.nlm.nih.gov/31921498><https://www.ncbi.nlm.nih.gov/pmc/articles/PMC6936633/>.
- [26] Maithra Raghu, Chiyuan Zhang, Jon Kleinberg, and Samy Bengio. Transfusion: Understanding transfer learning for medical imaging. In H. Wallach, H. Larochelle, A. Beygelzimer, F. d'Alché-Buc, E. Fox, and R. Garnett, editors, *Advances in Neural Information Processing Systems 32*, pages 3347–3357. Curran Associates, Inc., 2019. URL <http://papers.nips.cc/paper/8596-transfusion-understanding-transfer-learning-for-medical-imaging.pdf>.
- [27] A. Romero Lopez, X. Giro-i-Nieto, J. Burdick, and O. Marques. Skin lesion classification from dermoscopic images using deep learning techniques. In *2017 13th IASTED International Conference on Biomedical Engineering (BioMed)*, pages 49–54, 2017.
- [28] Veronica Rotemberg, Nicholas Kurtansky, Brigid Betz-Stablein, Liam Caffery, Emmanouil Chousakos, Noel Codella, Marc Combalia, Stephen Dusza, Pascale Guitera, David Gutman, Allan Halpern, Harald Kittler, Kivanc Kose, Steve Langer, Konstantinos Lioprys, Josep Malvehy, Shenara Musthaq, Jabpani Nanda, Ofer Reiter, George Shih, Alexander Stratigos, Philipp Tschandl, Jochen Weber, and H. Peter Soyer. A patient-centric dataset of images and metadata for identifying melanomas using clinical context, 2020.
- [29] Eiko Saito and Megumi Hori. Melanoma skin cancer incidence rates in the world from the Cancer Incidence in Five Continents XI. *Japanese Journal of Clinical Oncology*, 48(12): 1113–1114, 11 2018. ISSN 1465-3621. doi: 10.1093/jjco/hyy162. URL <https://doi.org/10.1093/jjco/hyy162>.
- [30] M. Sandler, A. Howard, M. Zhu, A. Zhmoginov, and L. Chen. Mobilenetv2: Inverted residuals and linear bottlenecks. 2019.

- [31] Karen Simonyan and Andrew Zisserman. Very deep convolutional networks for large-scale image recognition. *arXiv 1409.1556*, 09 2014.
- [32] Pascal Sturmfels, Scott Lundberg, and Su-In Lee. Visualizing the impact of feature attribution baselines. *Distill*, 5(1):e22, 2020. URL <https://distill.pub/2020/attribution-baselines/>.
- [33] Mukund Sundararajan, Ankur Taly, and Qiqi Yan. Axiomatic attribution for deep networks. In *Proceedings of the 34th International Conference on Machine Learning - Volume 70*, ICML’17, page 3319–3328. JMLR.org, 2017.
- [34] C. Szegedy, W. Liu, Y. Jia, P. Sermanet, S. Reed, D. Anguelov, D. Erhan, V. Vanhoucke, and A. Rabinovich. Going deeper with convolutions. 2014.
- [35] C. Tan, F. Sun, T. Kong, W. Zhang, C. Yang, and C. Liu. A survey on deep transfer learning. *Artificial Neural Networks and Machine Learning - ICANN 2018*, Lecture Notes in Computer Science, vol 11141:270–279, 2018. URL https://doi.org/10.1007/978-3-030-01424-7_27.
- [36] M. Tan, B. Chen, R. Pang, V. Vasudevan, Mark S., A. Howard, and Q. V. Le. Mnasnet: Platform-aware neural architecture search for mobile, 2019.
- [37] J.A. Wolf, J.F. Moreau, O. Akilov, J.C. English 3rd T. Patton, J. Ho, and L. K. Ferris. Diagnostic inaccuracy of smartphone applications for melanoma detection. 2013. doi: 10.1001/jamadermatol.2013.2382.
- [38] S. Xie, R. Girshick, P. Dollár, Z. Tu, and K. He. Aggregated residual transformations for deep neural networks, 2017.
- [39] L. Yu, H. Chen, Q. Dou, J. Qin, and P. Heng. Automated melanoma recognition in dermoscopy images via very deep residual networks. *IEEE Transactions on Medical Imaging*, 36(4): 994–1004, 2017.
- [40] Blazej Zbytek, J Andrew Carlson, Jacqueline Granese, Jeffrey Ross, Martin C Mihm Jr, and Andrzej Slominski. Current concepts of metastasis in melanoma. *Expert review of dermatology*, 3(5):569–585, oct 2008. ISSN 1746-9872. doi: 10.1586/17469872.3.5.569. URL <https://pubmed.ncbi.nlm.nih.gov/19649148><https://www.ncbi.nlm.nih.gov/pmc/articles/PMC2601641/>.
- [41] Hasib Zunair and A. Hamza. Melanoma detection using adversarial training and deep transfer learning. 04 2020.

A Transfer Learning Architectures

VGG VGG [31] is an advancement of a previous deep neural network, AlexNet [16]. The model uses small receptive fields of 3x3 with five max-pooling layers. In our paper, we use VGG16.

GoogleNet GoogleNet [34] was developed in 2014 to solve the problem of overfitting by building an Inception Module, using filters of multiple sizes. Three filter sizes of 1x1, 3x3, and 5x5 are simultaneously used; whereby the 1x1 convolution is used to shrink the dimensions of the model. The GoogleNet architecture consists of 9 Inception Modules, with each module connected to an average pooling layer.

ResNet ResNet [6] short for “Residual Network”, is a deep learning model developed in 2015 and was the winner of the ImageNet Competition [4]. In our research, we use ResNet50, a variant of the ResNet Model. The model consists of 48 Convolutional layers, 1 Max Pooling and 1 Average Pooling layer. ResNet addresses the vanishing-exploding gradients by leveraging skip connections for identity mapping, simplifying the network.

SqueezeNet SqueezeNet [11] uses fewer parameters while preserving similar performance to AlexNet [16]. There are several architectural features worth noting: the use of 1x1 convolution filters, decreased number of input channels, and down-sampling later in the network.

DenseNet DenseNet [10] is similar to the architecture of ResNet but with “DenseBlocks”. Each DenseBlock consists of a convolution layer, pooling layer, batch normalisation, and non-linear activation layer.

ResNeXt Built on the Residual Network and VGG, ResNeXt [38] uses a similar split-transform-merge strategy with an additional cardinality dimension (size of a set of transformations). The model borrows the repeating layers strategy from VGG and ResNet and according to the researchers, has better performance than ResNet [6] but with only 50% complexity.

MobileNet MobileNet [30] was developed for devices with smaller computational power such as smartphones. Unlike bigger deep learning networks such as VGG, MobileNet uses depthwise separable convolution, performing convolution on the input channels separately and then by pointwise convolution. This way low latency models can be developed, which are applicable to mobile devices.

ShuffleNet ShuffleNet [19] was also designed for mobile devices with small computational power. The model uses 1x1 convolution and channel shuffle, designed specifically for small networks. ShuffleNet has efficient computation while obtaining an accuracy similar to and thirteen times faster than AlexNet [16].

MnasNet MnasNet [36] is another mobile network designed for efficient performance using a multi-objective neural architecture search approach that considers accuracy and latency. The network also uses a hierarchical search space, achieving speeds faster than MobileNet [30].

EfficientNet EfficientNet [18] is a recent mobile network developed in 2018, which applies a compound coefficient for improved accuracy. Rather than scaling up the CNN model by an arbitrary amount, the authors use a grid search to find correlation in scaling based on the AutoML neural architecture search.

B Hyperparameter Optimisation

For the standard CNN model, values in a range were tested for dropout, batch size, kernel size, learning rate, number of layers, pool size, and number of convolution filters using random search, which is a more efficient method of hyperparameter optimisation than grid or manual search [12]. The search ranges and final values are shown in Table 2.

Hyperparameter	Value	Lower	Upper	Scale
Dropout	0.4	0.0	0.5	Linear
Batch Size	8	4	512	\log_2
Kernel Size	4	2	5	Linear
Learning Rate	0.00977	0.001	0.01	\log_{10}
Number of Layers	5	5	10	Linear
Pool Size	3	3	4	Linear
Convolution Filters	11	6	12	Linear

Table 2: Hyperparameter search ranges and final values.

C Implementation

All deep learning methods were implemented in PyTorch [24] and were optimised using Adam [14]. The models were trained using Tesla P100 GPUs. Each model was trained over 10 independent training runs with early stopping [17] for a maximum of 15 epochs (the patience constant was set to 3). We used step decay in the learning rate (the decay was set to 0.4 with a learning patience of 1).

D Additional Tables and Figures

Location	Normal	Melanoma
Torso	17106	257
Lower extremity	8293	124
Upper extremity	4872	111
Head/neck	1781	74
Palms/soles	370	5
Oral/genital	120	4

Table 3: Distribution of normal and melanoma skin lesion samples based on location of body.